AJNR

Normal Cranial Nerves in the Cavernous Sinuses: Contrast-Enhanced Three-Dimensional Constructive Interference in the Steady State MR Imaging

Akiko Yagi, Noriko Sato, Ayako Taketomi, Takahito Nakajima, Hideo Morita, Yoshinori Koyama, Jun Aoki and Keigo Endo

AJNR Am J Neuroradiol 2005, 26 (4) 946-950
http://www.ajnr.org/content/26/4/946

Normal Cranial Nerves in the Cavernous Sinuses: Contrast-Enhanced Three-Dimensional Constructive Interference in the Steady State MR Imaging

Akiko Yagi, Noriko Sato, Ayako Taketomi, Takahito Nakajima, Hideo Morita, Yoshinori Koyama, Jun Aoki, and Keigo Endo

BACKGROUND AND PURPOSE: **Three-dimensional (3D) constructive interference in steady state (CISS) MR imaging is useful for demonstrating cranial nerves (CNs) in the cistern. The purpose of this study was to evaluate normal CNs III, IV, V_1, V_2, and VI in the cavernous sinuses by using contrast-enhanced, three-dimensional (3D), Fourier transformation CISS MR imaging.**

METHODS: **In 76 normal cavernous sinuses from 38 patients, detectability of CNs III–VI in the bilateral cavernous sinuses was evaluated by using contrast-enhanced 3D CISS MR imaging. In 40 cavernous sinuses from 20 patients, contrast-enhanced 3D CISS and contrast-enhanced T1-weighted MR imaging were compared for the detectability of these CNs.**

RESULTS: **Each CN was separately demonstrated, and in 11 patients (29%), all CNs in the cavernous sinuses were identified on contrast-enhanced 3D CISS MR imaging. The images depicted the intracavernous segments of CNs III, IV, V_1, V_2, and VI in 76 (100%), 46 (61%), 70 (92%), 67 (88%), and 73 (96%) of the 76 sinuses, respectively. In comparison of imaging techniques, contrast-enhanced 3D CISS MR imaging had a detection rate significantly higher than that of enhanced T1-weignting imaging ($P < .05$) in all CNs except for CN III, which was detected in 100% of cases with both techniques.**

CONCLUSION: **Contrast-enhanced 3D CISS MR imaging provides clear images of each CN in the cavernous segment. This useful method may contribute to the diagnosis of diseases involving the cavernous sinuses, such as Tolosa-Hunt syndrome.**

The cavernous sinus contains the venous plexus, internal carotid artery (ICA), periarterial sympathetic nerve fibers, fibrous tissue and cranial nerves (CNs) III (oculomotor nerve), IV (trochlear nerve), V_1 (ophthalmic nerve), V_2 (maxillary nerve), and VI (abducens nerve). Given the inclusion of these major vessels and nerves, the cavernous sinus is a clinically important structure. Visualization of CNs III, IV, V_1, V_2, and VI in the cavernous sinus has been reported with both MR imaging and CT (1–8). However, precise evaluation of these CNs in the cavernous sinus is difficult.

Received May 19, 2004; accepted after revision August 6.

From the Department of Diagnostic Radiology and Nuclear Medicine (A.Y., N.S., A.T., T.N., H.M., Y.K., J.A., K.E.), Gunma University School of Medicine, Gunma, Japan.

Address reprints request to Noriko Sato, M.D., Ph.D., Department of Diagnostic Radiology and Nuclear Medicine, Gunma University School of Medicine, 3–39-15 Showa-machi, Maebashi Gunma, 371-8511, Japan.

Three-dimensional (3D) constructive interference in steady state (CISS) is a high spatial–resolution, refocused, gradient-echo sequence that is flow compensated. The 3D CISS sequence depicts small structures surrounded by CSF with high contrast and high spatial resolution; therefore, it is suitable for depicting CNs in the cistern. 3D CISS gives the appearance of a heavily T2-weighted sequence. Because the contrast of CISS sequence is proportional to T2 relaxation time/T1 relaxation time, CSF signal intensity on CISS imaging is higher than that of brain parenchyma. Therefore, CISS images have an appearance similar to that of T2-weighted images. However, 3D CISS sequences show increased contrast as concentration of gadolinium-based contrast agent increases (9). We found that CNs III, IV, V_1, V_2, and VI in the cavernous sinus were well demonstrated in vivo on 3D CISS imaging after the injection of gadodiamide hydrate, with the well-enhanced venous plexus of the cavernous sinus playing a similar role to CSF. Using this new method, we studied the normal anatomy in

the cavernous sinus and evaluated the detectability of each CN on both contrast-enhanced 3D CISS MR imaging and contrast-enhanced conventional T1-weighted MR imaging.

Methods

Patients

Detectability of intracavernous segments of CNs III, IV, V_1, V_2, and VI was evaluated on MR imaging in 76 normal cavernous sinuses. We examined 38 patients (13 men, 25 women; mean age, 51.2 years; range, 16–78 years) between June 2000 and April 2004. Their presentations and indications included acoustic schwannoma ($n = 11$); cholesteatoma ($n = 4$); screening for brain metastases in patients with thoracic or abdominal malignancies without other known metastasis ($n = 5$); benign nasal tumor (fibroma and schwannoma, $n = 2$); neurovascular compression of a facial nerve ($n = 3$); Rathke cleft cyst ($n = 2$); temporal bone cyst ($n = 1$); middle ear adenoma ($n = 1$); pineal cyst ($n = 1$); pituitary screening ($n = 2$); and screening for auditory disturbance, tinnitus, or dizziness ($n = 6$). All patients were free of neurologic symptoms for CNs III–VI and had not received chemotherapy or radiation therapy. No patients had paranasal sinusitis. Eleven patients with acoustic schwannoma had undergone surgical resection 3–24 months earlier, without recurrence. Tumor size before surgery was <10 mm in all 11 patients and did not involve CNs III–VI. Two patients who underwent pituitary screening had no abnormal MR findings. One was referred for an evaluation of an elevated serum thyroid stimulating hormone level due to antithyroid medication, and the other patient was referred for an evaluation of obesity. All patients being screened for auditory disturbance or tinnitus or dizziness had normal MR imaging results. All participants provided written informed consent before entering the study.

MR Imaging

All MR imaging examinations were performed by using a 1.5-T unit (Magnetom Symphony; Siemens, Erlangen, Germany) with a regular head coil. All patients underwent contrast-enhanced 3D CISS MR imaging for the evaluation of bilateral cavernous sinuses. Gadodiamide hydrate (Omniscan; Daiichi Pharmaceutical Co., Tokyo, Japan) was administered at a dose of 0.1 mmol/kg body weight as the intravenous contrast agent. In addition, 20 patients underwent contrast-enhanced coronal T1-weighted MR imaging. Two pulse sequences were used: 1) 3D CISS (TR/TE/NEX = 11.84/5.92/1, 70° flip angle, 180 × 180-mm (read × phase encode) FOV, 39.2-mm slab thickness, 256 × 224 matrix, 56 three-dimensional partitions, one slab, 0.7 × 0.8-mm pixel, 0.7-mm effective section thickness, and imaging time of 4 minutes 28 seconds, and 2) conventional coronal T1-weighted MR imaging (TR/TE = 450/15, 200 × 180-mm FOV, 320 × 202 matrix, 3.0-mm section thickness, 0-mm intersection gap).

Image Analysis

Data obtained by using 3D CISS MR imaging were reconstructed in coronal planes by using a section thickness of 0.7 mm. Images were analyzed with a multiplanar reconstruction program (Siemens). We compared the position of a given point in one plane with the same position in two other perpendicular planes. Two neuroradiologists (A.Y., N.S.) analyzed the images collaboratively. Each neuroradiologist made initial evaluations independently, and any disagreements regarding final conclusions were resolved by consensus. Normal CNs III–VI were identified in the cavernous sinus when a dark spot was observed in the appropriate location on more than three consecutive sections from contrast-enhanced CISS MR imaging and on more than one section from contrast-enhanced T1-weighted MR imaging. In addition, we confirmed the continuity of each nerve on reconstructed planes by following the course of each nerve to exclude false-positive results. When CNs were not identified, they were defined as not identified.

In 76 normal cavernous sinuses from 38 patients, detectability of intracavernous segments of CNs III–VI was examined by using contrast-enhanced 3D CISS MR imaging. To evaluate the influence of age, comparisons were made between two groups: those younger than 55 years and those older than 55 years. In 40 cavernous sinuses from 20 patients, the detectability of CNs III–VI was compared between contrast-enhanced CISS MR imaging and contrast-enhanced T1-weighted MR imaging.

Statistical Analysis

Statistical comparison of the detectability of CNs with both imaging techniques was performed by using the Fischer exact probability test. Statistical comparison of the detectability of CNs III–VI on contrast-enhanced 3D CISS MR imaging between the two age groups was also performed by using the Fischer exact probability test. $P < .05$ was considered to indicate a statistically significant correlation.

Results

Intracavernous segments of CNs III, IV, V_1, V_2, and VI were identified on contrast-enhanced 3D CISS MR imaging in 76 (100%), 46 (61%), 70 (92%), 67 (88%), and 73 (96%) of the 76 cavernous sinuses, respectively. In 11(29%) of 38 patients, all CNs in the cavernous sinus were identified (Fig 1). No significant differences in each nerve were observed between the younger group (six men, 13 women; age ≤ 55; mean age, 37.4 years) and the older group (seven men, 12 women; age >55 years; mean age, 64.9 years) (Table 1).

Our comparison of the detectability of the 40 cavernous sinuses showed that intracavernous segments of CNs III, IV, V_1, V_2, and VI were identified in 40 (100%), 26 (65%), 37 (93%), 35 (88%), and 38 (95%) cases on contrast-enhanced 3D CISS MR imaging, and in 40 (100%), 12 (30%), 18 (45%), 21 (53%), and 26 (65%) cases on contrast-enhanced T1-weighted MR imaging, respectively (Table 2). CN III was identified in all cases on both contrast-enhanced 3D CISS and contrast-enhanced T1-weighted MR imaging. However, significant differences were noted in all other CNs between the two imaging techniques. Enhanced 3D CISS MR imaging was superior to enhanced T1-weighted MR imaging in depicting the CNs in the cavernous portions (Fig 2).

Discussion

The anatomy of the cavernous sinus has been studied on dissections and is well explored (10–17). CN III lies superolateral to the ICA, and CN IV is inferior to CN III. CN V_1 courses inferolateral to the upper portion of the ICA siphon, and CN V_2 runs in the inferolateral aspect of the cavernous sinus. CN VI is the only CN to run inside the cavernous sinus, lateral to the ICA.

Some groups have reported cavernous sinus structures on MR imaging (1–4, 18). One of them evaluated the detectability of CNs in the normal cavernous

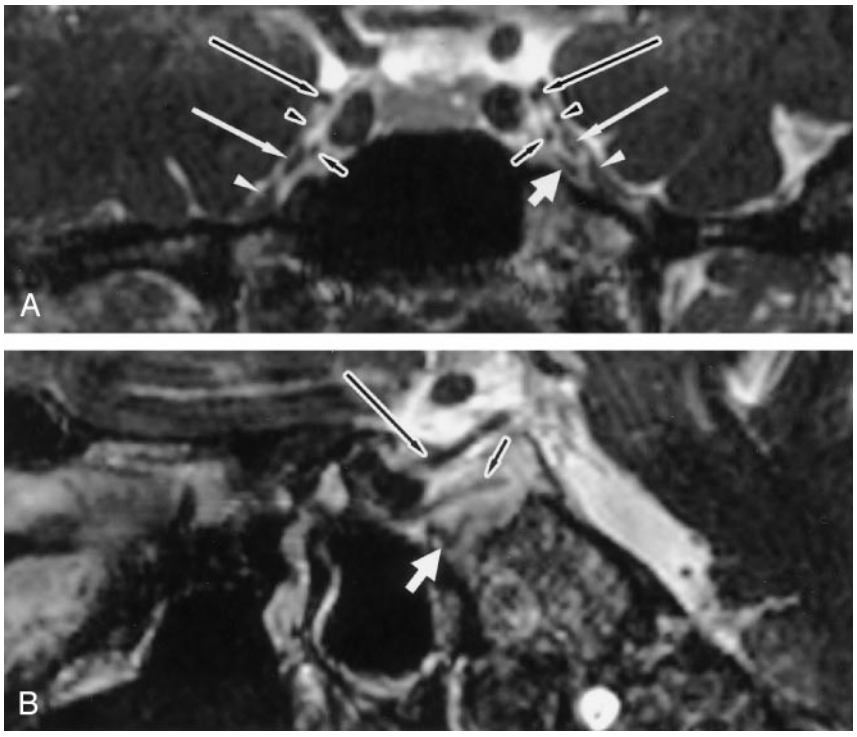

FIG 1. Contrast-enhanced CISS MR images (TR/TE = 11.8/5.9) in a 44-year-old woman whose acoustic schwannoma had been resected without recurrence.

A, Coronal view clearly shows bilateral CNs III (*long black arrow*), IV (*black arrowhead*), V_1 (*long white arrow*), V_2 (*white arrowhead*), and VI (*short black arrow*) are clearly demonstrated in the normal cavernous sinuses. Additional dark spot is shown inferior to left CNs V_1 and VI (*short white arrow*).

B, Oblique sagittal view also depicts the left CNs III (*long black arrow*) and VI (*short black arrow*) well. Additional dark region shown in *A* is also identified as a serpiginous, dark line without continuity (*short white arrow*). It is considered to be fibrous tissue.

TABLE 1: Detectability of cranial nerves in patients with normal cavernous sinuses on enhanced 3D CISS MR imaging

	CN				
Patients	III	IV	V_1	V_2	VI
16–55 y (n = 38)*	38 (100)	24 (63)	36 (95)	32 (84)	38 (100)
56–78 y (n = 38)†	38 (100)	22 (58)	34 (89)	35 (92)	35 (92)
P value		.815	.674	.480	.240

Note.—Data are the number of nerves identified. Data in parentheses are percentages.

* Mean age, 37.4 y.

† Mean age, 64.9 y.

TABLE 2: Detectability of cavernous segments of cranial nerves in 40 normal cavernous sinuses on enhanced imaging

Contrast-Enhanced Imaging	CN				
	III	IV	V_1	V_2	VI
CISS (n = 40)	40 (100)	26 (65)	37 (93)	35 (88)	38 (95)
T1 weighted (n = 40)	40 (100)	12 (30)	18 (45)	21 (53)	26 (65)
P value		.003	<.001	.001	.001

Note.—Data are the number of nerves identified. Data in parentheses are percentages.

sinuses. Korogi et al (4) studied dynamic contrast-enhanced MR imaging of the cavernous sinus. In their study, CNs III and IV were defined as a single anatomic structure, as were V_1 and VI. On dynamic MR imaging, CNs III and IV, V_1 and VI, and V_2 all had a detectability rate of 75%. On conventional contrast-enhanced MR imaging, the detectability rates were 62%, 30%, and 28%, respectively. We believe that CN V_1 and VI should be distinguished, even on contrast-enhanced T1-weighted MR imaging, because their anatomic courses in the cavernous sinus differ, as we have shown. To our knowledge, no imaging study has been undertaken to precisely evaluate the CNs in the cavernous sinus in vivo, and we may be the first to demonstrate them clearly and separately.

Casselman et al (19) introduced the 3D CISS sequence to visualize CNs in the internal acoustic canal and at the cerebellopontine angle. The 3D CISS sequence has been used to demonstrate various other CNs (20–27). Yousry et al (22) used the 3D CISS sequence to show that 11 of the 12 CNs in their cisternal course were always (100%) identified with a high degree of certainty, with only CN IV varying in cisternal course and being identified in just 47.5% of cases.

To our knowledge, no studies have demonstrated CNs III–VI in the cavernous sinus on CISS MR imaging. Shigematsu et al (9) reported that, although 3D CISS gives the appearance of a heavily T2-weighted sequence, 3D CISS sequences show increased contrast as concentration of gadolinium-based contrast agent increases. Our study showed that CNs III, IV, V_1, V_2, and VI in the cavernous sinus were well visualized on contrast-enhanced 3D CISS MR imaging, with the enhanced venous plexus playing a role similar to CSF. Venous spaces in the cavernous sinus were strongly enhancing, and CNs were shown as nonenhanced spots of hypointensity. In a previous study, it was not possible to detect each CN separately. On the contrarily, we visualized each nerve clearly for the first time. Detectability rates for CNs III, IV, V_1, V_2, and VI in the cavernous sinus were 100%, 61%, 92%, 88%, and 96%, respectively, on contrast-enhanced CISS MR imaging. These detectability rates are higher than those of the previous

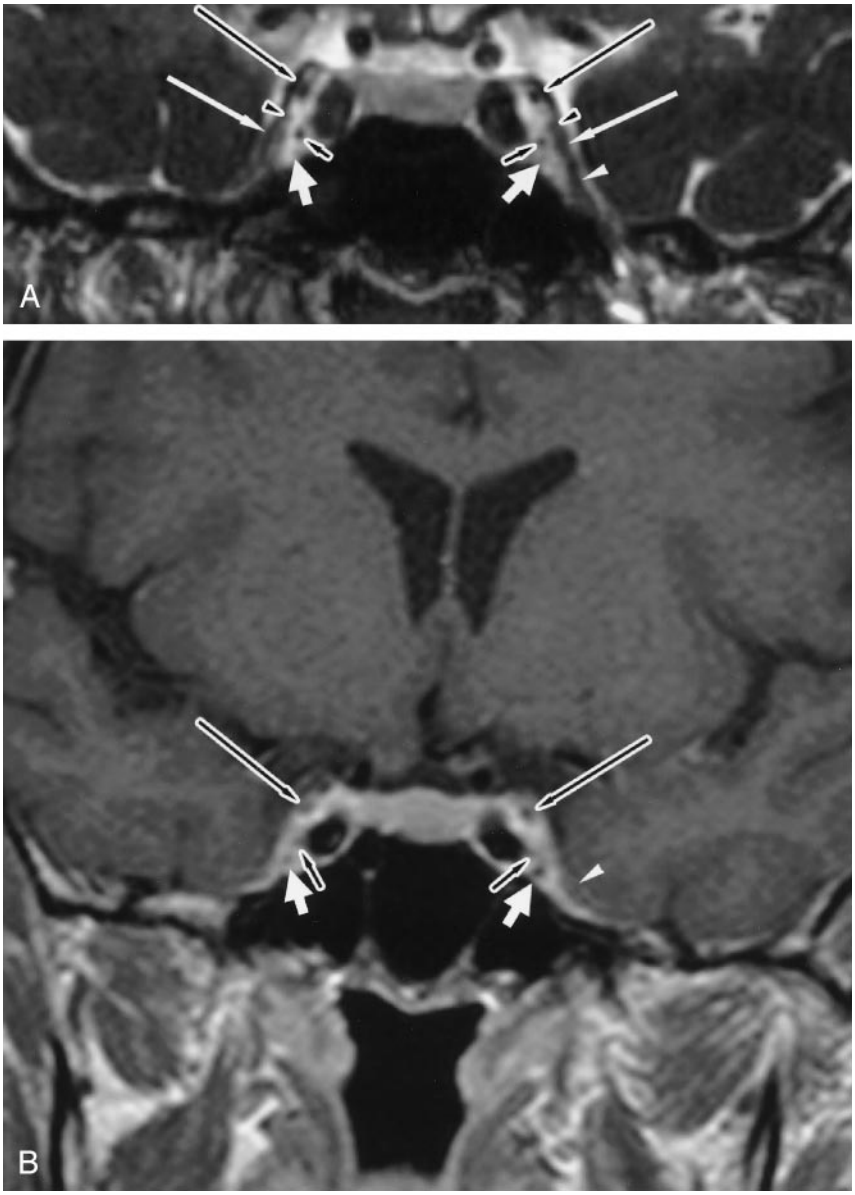

FIG 2. Normal cavernous sinuses in a 46-year-old woman after surgical resection of left acoustic schwannoma without recurrence.

A, Enhanced coronal CISS MR image (TR/TE = 11.8/5.9) shows bilateral CNs III (*long black arrows*), IV (*black arrowheads*), V_1 (*long white arrows*), left V_2 (*white arrowhead*), and bilateral VI (*short black arrows*). Only the right CN V_2 is not identified. Additional faint, low-intensity spots are inferior to CNs VI (*short white arrows*), which are not considered to be nerves because they are in an anatomically different location and because they do not have continuity on reconstructed CISS MR imaging.

B, Enhanced coronal T1-weighted MR image (TR/TE = 450/15) shows only bilateral CNs III (*long black arrow*), left CN V_2 (*white arrowhead*), and bilateral CNs VI (*short black arrow*).Other small contrast defects are just inferior to the bilateral CN VI (*short white arrows*), as shown in *A*.

study (4). We compared detectability between contrast-enhanced CISS and contrast-enhanced T1-weighted MR imaging and found that it was predominantly and significantly higher with the former than with the latter.

CN III is large and was identified on both contrast-enhanced CISS and contrast-enhanced T1-weighted MR imaging at a rate of 100%. In a previous report, CN IV in the cavernous sinus could not be individually discriminated because of its small size and proximity to CN III (18). However, contrast-enhanced CISS MR imaging depicted CN IV in 61% of cases. We found that CN IV did not always run near CN III and sometimes ran near CN V_1. van Overbeeke et al (16) reported that, in 75% of their dissections, CN IV was near to CN III; in the other 25%, the nerve was closer to CN V_1. Detectability of CNs V_1 and V_2 was high in our study. V_2 is reportedly easy to identify during routine head MR imaging, given its exit from the skull through the foramen rotundum (18). Indeed, in our study, V_2 was easily identified. However, when it was flattened and tightly attached to the dura matter, its differentiation from dura was sometimes difficult. CN VI was second only to CN III in terms of detectabilty, because of its characteristic course inside the cavernous sinus.

On contrast-enhanced CISS MR imaging, some nonenhanced areas were observed in addition to CNs. These were considered to correspond to periarterial sympathetic fibers, fibrous tissues, or branches of the ICA. From the intracavernous segment of the ICA, two main branches arise, the meningohypophyseal trunk and the inferior lateral trunk. The three main branches of the meningohypophyseal trunk are the tentorial artery, the dorsal meningeal artery, and the inferior hypophyseal artery (10). Branches of CN VI were also considered responsible for some nonenhanced structures. Harris and Rhoton (10) found that the abducens nerve does not always represent a single trunk in the cavernous sinus, and it frequently splits

into multiple rootlets numbering anywhere from two to five. Ozveren et al (28) stated that, in autopsy materials, four of 50 cases had a duplicated bilateral abducens nerves, and seven of 50 cases had duplicated unilateral abducens nerves. We distinguished the CNs from other structure on the oblique view that was reconstructed during 3D CISS MR imaging (eg, Fig 1B).

Conclusion

Contrast-enhanced 3D CISS MR imaging offers clear images of normal CNs in the cavernous sinus, which has not been shown in vivo. In the comparative study between contrast-enhanced CISS and contrast-enhanced T1-weighted MR imaging, the former offered significantly higher detectability of CNs. Contrast-enhanced 3D CISS MR imaging is a useful method, one that will contribute to the diagnosis of diseases involving cavernous sinuses, such as Tolosa-Hunt syndrome.

Acknowledgments

We thank Kazuo Takeuchi, MD, MPH, PhD, from Takasaki University of Health and Welfare, for his support in the statistical analysis in the present study.

References

1. Daniels DL, Pech P, Mark L, Pojunas K, Williams AL, Haughton VM. **Magnetic resonance imaging of the cavernous sinus.** *AJR Am J Roentgenol* 1985;144:1009–1014
2. Hirsch WL Jr, Hryshko FG, Sekhar LN, et al. **Comparison of MR imaging, CT, and angiography in the evaluation of the enlarged cavernous sinus.** *AJNR Am J Neuroradiol* 1988;9:907–915
3. Daniels DL, Czervionke LF, Bonneville JF, et al. **MR imaging of the cavernous sinus: value of spin echo and gradient recalled echo images.** *AJNR Am J Neuroradiol* 1988;9:947–952
4. Korogi Y, Takahashi M, Sakamoto Y, Shinzato J. **Cavernous sinus: correlation between anatomic and dynamic gadolinium-enhanced MR imaging findings.** *Radiology* 1991;180:235–237
5. Caillet H, Delvalle A, Doyon D, et al. **Visibility of cranial nerves at MRI.** *J Neuroradiol* 1990;17:289–301
6. Laine FJ. **Cranial nerves III, IV, and VI.** *Top Magn Reson Imaging* 1996;8:111–130
7. Casselman JW, Dehaene I. **Imaging of the IIIrd, IVth, and VIth cranial nerves.** *Neuroophthalmology* 1998;19:63–68
8. Eisenkraft B, Ortiz AO. **Imaging evaluation of cranial nerves 3, 4, and 6.** *Semin Ultrasound CT MRI* 2001;22:488–501
9. Shigematsu Y, Korogi Y, Hirai T, et al. **Contrast-enhanced CISS MRI of vestibular schwannomas: phantom and clinical studies.** *J Comput Assist Tomogr* 1999;23:224–231
10. Harris FS, Rhoton AL Jr. **Anatomy of the cavernous sinus: a microsurgical study.** *J Neurosurg* 1976;45:169–180
11. Umansky F, Nathan H. **The lateral wall of the cavernous sinus.** *J Neurosurg* 1982;56:228–234
12. Taptas JN. **The so-called cavernous sinus: a review of the controversy and its implications for neurosurgeons.** *Neurosurgery* 1982;11:712–717
13. Ono M, Ono M, Rhoton AL Jr, Barry M. **Microsurgical anatomy of the region of the tentorial incisura.** *J Neurosurg* 1984;60:365–399
14. Kehrli P, Ali M, Reis M Jr, et al. **Anatomy and embryology of the lateral sellar compartment (cavernous sinus) medial wall.** *Neurol Res* 1998;20:585–592
15. Dietemann JL, Kehrli P, Maillot C, et al. **Is there a dural wall between the cavernous sinus and the pituitary fossa? Anatomical and MRI findings.** *Neuroradiology* 1998;40:627–630
16. van Overbeeke JJ, Jansen JJ, Tulleken CA. **The cavernous sinus syndrome: an anatomical and clinical study.** *Clin Neurol Neurosurg* 1988;90:311319
17. Tuccar E, Uz A, Tekdemir I, Elhan A, Ersoy M, Deda H. **Anatomical study of the lateral wall of the cavernous sinus, emphasizing dural construction and neural relations.** *Neurosurg Rev* 2000;23:45–48
18. Castillo M. **Imaging of the upper cranial nerves I, III-VIII, and the cavernous sinuses.** *Magn Reson Imaging Clin N Am* 2002;10:415–431
19. Casselman JW, Kuhweide R, Deimling M, Ampe W, Dehaene I, Meeus L. **Constructive interference in steady state-3DFT MR imaging of the inner ear and cerebellopontine angle.** *AJNR Am J Neuroradiol* 1993;14:47–57
20. Held P, Fellner C, Fellner F, Seitz J, Strutz J. **MRI of inner ear anatomy using 3D MP-RAGE and 3D CISS sequences.** *Br J Radiol* 1997;70:465–472
21. Lemmerling M, De Praeter G, Mortelé K, et al. **Imaging of the normal pontine cisternal segment of the abducens nerve, using three-dimensional constructive interference in the steady state MRI.** *Neuroradiology* 1999;41:384–386
22. Yousry I, Camelio S, Schmid UD, et al. **Visualization of cranial nerves I-XII: value of 3D CISS and T2-weighted FSE sequences.** *Eur Radiol* 2000;10:1061–1067
23. Held P, Nitz W, Seitz J, et al. **Comparison of 2D and 3D MRI of the optic and oculomotor nerve anatomy.** *Clin Imaging* 2000;24:337–343
24. Held P, Fründ R, Seitz J, Nitz W, Haffke T, Hees H. **Comparison of 2-D turbo spin echo and 3-D gradient echo sequences for the detection of the trigeminal nerve and branches anatomy.** *Eur J Radiol* 2001;37:18–25
25. Seitz J, Held P, Strotzer M, et al. **MR imaging of cranial nerve lesions using six different high-resolution T1- and T2(*)-weighted 3D and 2D sequences.** *Acta Radiol* 2002;43:349–353
26. Yousry I, Moriggl B, Dieterich M, Naidich TP, Schmid UD, Yousry TA. **MR anatomy of the proximal cisternal segment of the trochlear nerve: neurovascular relationships and landmarks.** *Radiology* 2002;223:31–38
27. Yousry I, Camelio S, Wiesmann M, et al. **Detailed magnetic resonance imaging anatomy of the cisternal segment of the abducent nerve: Dorello's canal and neurovascular relationships and landmarks.** *J Neurosurg* 1999;91:276–283
28. Ozveren MF, Sam B, Akdemir I, Alkan A, Tekdemir I, Deda H. **Duplication of the abducens nerve at the petroclival region: an anatomic study.** *Neurosurgery* 2003;52:645–652